Available online at www.sciencedirect.com
SCIENCE DIRECT®
International Journal of Heat and Mass Transfer 47 (2004) 203–214
International Journal of HEAT and MASS TRANSFER
www.elsevier.com/locate/ijhmt

Optimal distribution of discrete heat sources on a wall with natural convection

A.K. da Silva [a], S. Lorente [b], A. Bejan [a,*]

[a] Department of Mechanical Engineering and Materials Science, Duke University, Box 90300, Durham, NC 27708-0300, USA
[b] Department of Civil Engineering, National Institute of Applied Sciences (INSA), 135 Avenue de Rangueil, Toulouse 31077, France

Received 18 April 2003; received in revised form 30 July 2003

Abstract

This paper is an application of the constructal method to the discovery of the optimal distribution of discrete heat sources cooled by laminar natural convection. The global objective is to maximize the global conductance between the wall and the fluid, or to minimize the hot-spot temperatures when the total heat generation rate and global system dimensions are specified. Two scenarios are investigated: (i) a large number of small heat sources mounted on a vertical wall facing a fluid reservoir, and (ii) a small number of finite-size heat sources mounted on the inside of the side wall of a two-dimensional enclosure. It is shown that the optimal distribution is not uniform (the sources are not equidistant), and that as the Rayleigh number increases the heat sources placed near the tip of a boundary layer should have zero spacings. In both (i) and (ii), the optimal configuration of the wall with discrete sources is generated by the pursuit of maximal global performance subject to global constraints.

Keywords: Constructal theory; Electronics cooling; Packing; Enclosure; Natural convection; Discrete heat sources

1. Introduction

Making a better design has always been the goal in engineering. A valuable first step is to understand what 'better' means, that is, to see the objective of maximizing global performance, and to feel the global "finiteness" constraints. This step must be made early, before the system configuration (the design) has taken shape. This step frees the designer to think of an infinity of eligible configurations, or to imagine a configuration that 'morphs' freely. Better and better configurations are generated (not assumed), as global performance is pursued under constraints.

This unbiased way of approaching the discovery of optimal configuration is constructal theory and design [1]. It is particularly timely and relevant as we look ahead, because our computational tools continue to improve. It is becoming progressively easier and cheaper to simulate and evaluate flow architectures with many degrees of freedom. Such freedom was not available in the past, which is why until recently the 'better' designer was the one who had the intuition to "assume" only one or two clever configurations. Brilliance in innovation pushed performance upward, but kept design at the level of "art".

The future promises a design activity of a different kind—design as science, where freely morphing flow structures compete for performance, under the same constraints. Anything goes—all possible designs are eligible competitors, and the competition never ends. In engineering, the end is brought about by economics, and is known as the point of diminishing returns. In nature, the competition is permanent (e.g., river basins and animals continue to morph and improve), however, it is jolted by changes in the constraints, which redefine (displace, mutate) the search for the best.

In heat transfer, there is a growing body of work that illustrates the constructal method. The recent book review [1] shows numerous examples of optimized internal

* Corresponding author. Tel.: +1-919-660-5309; fax: +1-919-660-8963.
E-mail address: dalford@duke.edu (A. Bejan).

0017-9310/$ - see front matter © 2003 Elsevier Ltd. All rights reserved.
doi:10.1016/j.ijheatmasstransfer.2003.07.007

Nomenclature

c_p	specific heat, J/kg K
C	global conductance, Eq. (32)
D	heat source size, m
g	gravity, m s^{-2}
H	height, m
k	thermal conductivity, W m^{-1} K^{-1}
L	width, m
n	iteration number, Eq. (29)
N	total number of heat sources
N'	number of heat sources per unit of length, m^{-1}
P	pressure, Pa
Pr	Prandtl number
q'	heat transfer rate per unit length, W m^{-1}
q''	heat flux, W m^{-2}
q'''	heat transfer density, W m^{-3}
Q'	total heat transfer rate per unit length, W m^{-1}
R	residual vector
S	heat source spacing, m
Ra	Rayleigh number, Eq. (8)
Ra_*	Rayleigh number based on heat source strength, Eq. (24)
T	temperature, K
u	horizontal velocity component, m s^{-1}
u	solutions vector
v	vertical velocity component, m s^{-1}
x, y	Cartesian coordinates, m
y_0	continuously heated region, m

Greek symbols

α	thermal diffusivity, m^2 s^{-1}
β	coefficient of volumetric thermal expansion, K^{-1}
ρ	density, kg m^{-3}
ν	kinematic viscosity, m^2 s^{-1}
μ	viscosity, kg s^{-1} m^{-1}

Subscripts

$0, 1, \ldots, N$	heat source index
max	maximum when $N = 1$
2m	maximum when $N = 2$
3m	maximum when $N = 3$

Superscripts

i	trial mesh
$(\sim)$	dimensionless variables

structure (spacings) for assemblies cooled by natural convection or forced convection. The global objective is the maximization of heat transfer density, or the minimization of the hot-spot temperatures when the total heat generation rate, volume and other constraints are specified. Compactness, miniaturization, and multi-scale flow structures are generated along this route.

In the present paper we apply the constructal method to a fundamental problem in the cooling of electronics packages: the optimal positioning of discrete heat sources in a fixed volume with natural convection. The performance of packages with equidistant discrete heat sources was studied numerically and experimentally on a case by case basis [2–16]. The opportunity to optimize the positions of concentrated heat sources was recognized in Refs. [9,12]. The present work examines this opportunity in two settings: (i) a large number of small heat sources distributed freely on a vertical wall, and (ii) a small number of finite-size heat sources mounted freely inside one vertical all of a two-dimensional enclosure.

2. Large number of line heat sources

Consider a vertical wall of height H, which is in contact with a fluid reservoir of temperature T_∞ (Fig. 1). The wall is heated by horizontal line heat sources. Each

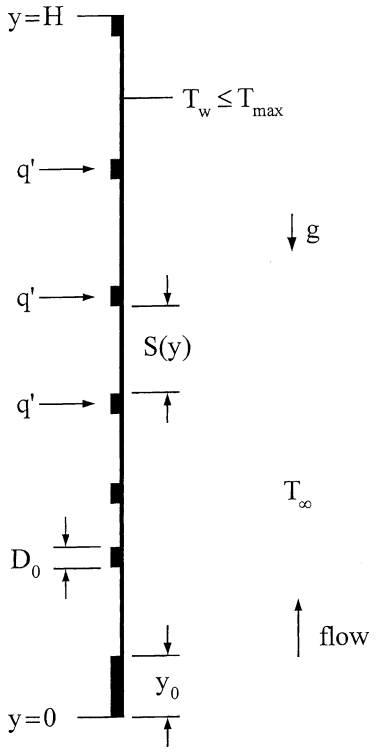

Fig. 1. The multiple length scales of the nonuniform distribution of finite-size heat sources on a vertical wall.

source has the strength q' [W/m]. The heat sources appear as points on the wall sketched in Fig. 1. Each line heat source extends in the direction perpendicular to the figure. The flow is two-dimensional and by natural convection in the boundary layer regime. The number of sources per unit of wall height is $N'(y)$,

$$N' = \frac{\text{number of sources}}{\text{unit height}} \tag{1}$$

According to constructal design, the global system (the wall) will perform best when all its elements work as hard as the hardest working element [1]. This means that if $T_{\max}$ is the maximal temperature that must not be exceeded at the hot-spots that occur on the wall, then the entire wall should operate at $T_{\max}$. The problem is to determine the distribution of heat sources on the wall, $N'(y)$, such that the wall temperature is near the allowed limit,

$$T_w(y) \cong T_{\max}, \quad \text{constant} \tag{2}$$

Assume that the density of line sources is sufficiently high so that we may regard the distribution of discrete q' sources as a nearly continuous distribution of nonuniform heat flux,

$$q''(y) = q'N' \tag{3}$$

The heat flux distribution that corresponds to Eqs. (2) and (3) and $Pr \gtrsim 1$ is [17]:

$$Nu \cong 0.5Ra_y^{1/4} \tag{4}$$

or, more explicitly,

$$\frac{q''}{T_{\max}-T_\infty}\frac{y}{k} \cong 0.5\left[\frac{g\beta(T_{\max}-T_\infty)y^3}{\alpha\nu}\right]^{1/4} \tag{5}$$

By eliminating $q''(y)$ between Eqs. (3) and (5) we obtain the required distribution of heat sources:

$$N'(y) \cong 0.5\frac{k}{q'}(T_{\max}-T_\infty)^{5/4}\left(\frac{g\beta}{\alpha\nu}\right)^{1/4} y^{-1/4} \tag{6}$$

This function shows that the heat sources must be positioned closer when they are near the start of the boundary layer. They must be farther apart on sections of the wall near $y = H$. The total number of q' sources that must be installed according to Eq. (6) on the wall of height H is

$$N = \int_0^H N'\mathrm{d}y \cong \frac{2}{3}\frac{k}{q'}(T_{\max}-T_\infty)Ra^{1/4} \tag{7}$$

where

$$Ra = \frac{g\beta H^3(T_{\max}-T_\infty)}{\alpha\nu} \tag{8}$$

The Rayleigh number is a dimensionless parameter that accounts for two global constraints, the wall height H and the maximal allowable excess temperature at the hot-spots. The total heat transfer rate from the q' sources to the T_∞ fluid is

$$Q' = q'N \cong \frac{2}{3}k(T_{\max}-T_\infty)Ra^{1/4} \tag{9}$$

This represents the global performance level to which any of the optimized nonuniform distributions of concentrated heat sources will aspire.

3. Heat sources with finite height

The physical implementation of the preceding results begins with the observation that the smallest scale that can be manufactured in the heating scheme of Fig. 1 is the D_0 height of the line heat source. The local spacing between two adjacent lines is $S(y)$. This spacing varies with altitude in accordance with the N' distribution function (6). The wall height interval that corresponds to a single line heat source is $D_0 + S(y)$. This means that the local number of heat sources per unit of wall height is

$$N'(y) = \frac{1}{D_0 + S(y)} \tag{10}$$

The heat strength of one source (q') is spread uniformly over the finite height of the source, $q_0'' = q'/D_0$. The heat flux q_0'' is a known constant, unlike the function $q''(y)$ of Eq. (5), which will be the result of design. By eliminating $N'(y)$ between Eqs. (6) and (10) we obtain the rule for how the wall heating scheme should be constructed:

$$\frac{S(y)}{H} \cong \frac{2q'Ra^{-1/4}}{k(T_{\max}-T_\infty)}\left(\frac{y}{H}\right)^{1/4} - \frac{D_0}{H} \tag{11}$$

The S function (11) has negative values in the vicinity of the start of the boundary layer. The smallest physical value that S can have is 0. This means that there is a starting wall section ($0 < y < y_0$) over which the line sources should be mounted flush against each other. The height of this section (y_0) is obtained by setting $S = 0$ and $y = y_0$ in Eq. (11).

$$\frac{y_0}{H} \cong Ra\left(\frac{D_0}{H}\right)^4\left[\frac{k(T_{\max}-T_\infty)}{2q'}\right]^4 \tag{12}$$

From $y = 0$ to $y = y_0$, the wall is heated with uniform flux of strength $q_0'' = q'/D_0$. The number of infinite-height sources that cover the height y_0 is $N_0 = y_0/D_0$. Above $y = y_0$ the wall is heated on discrete patches of height D_0, and the spacing between patches increases with height.

These basic features of the optimal design are illustrated in Fig. 1. The design has multiple length scales: H, D_0, y_0 and $S(y)$. The first two are constraints. The last two are interrelated, and are results of global maximization of performance, subject to the constraints. Taken

together, the lengths represent the constructal design—the flow architecture that (out of an infinity of possible architectures) brings the entire wall to the highest performance level possible.

The global heat transfer performance of the optimal design can be estimated in the limit where the number of heat-source strips D_0 is sufficiently large. In this limit, the integral (7) applies only in the upper region of the wall ($y_0 < y < H$), where the concentrated sources are spaced optimally according to Eq. (6). In the lower region of height y_0, the D_0 strips are mounted without spacings between them, and their number is

$$N_0 = \frac{y_0}{D_0} = Ra\left(\frac{D_0}{H}\right)^3\left(\frac{k(T_{\max}-T_\infty)}{2q'}\right)^4 \tag{13}$$

The total number of D_0 strips on the H wall is

$$N = N_0 + \int_{y_0}^{H} N'\mathrm{d}y = \frac{2}{3}\frac{k}{q'}(T_{\max}-T_\infty)Ra^{1/4}\left[1-\frac{3}{16}\left(\frac{k(T_{\max}-T_\infty)}{2q'}\right)^3 \times\left(\frac{D_0}{H}\right)^3 Ra^{3/4}\right] \tag{14}$$

This expression shows that in the limit $D_0 \to 0$, where the D_0 strips become line heat sources, Eq. (14) reduces to the simpler form shown in Eq. (7).

The total rate of heat transfer from the wall to the fluid is $Q' = q'N$, which yields

$$Q' \cong \frac{2}{3}k(T_{\max}-T_\infty)Ra^{1/4}\left[1-\frac{3}{16}\left(\frac{k(T_{\max}-T_\infty)}{2q'}\right)^3 \times\left(\frac{D_0}{H}\right)^3 Ra^{3/4}\right] \tag{15}$$

By comparing Eq. (15) with Eq. (9), we see that when D_0 is finite the total heat transfer rate is less than in the limit of line heat sources ($D_0 = 0$).

In summary, Eq. (15) is the more general, and represents the maximal performance of all the designs that are possible in the limit of large N. The optimization has already been performed, and is expressed by the optimal distribution shown in Eq. (6). This is why the only parameters that may still affect the global performance are visible in Eq. (15): they are the constraints, $(T_{\max}-T_\infty)$, H, D_0 and q'.

4. Heat sources on the wall of an enclosure

The more realistic configuration that serves as model for how the optimally distributed heat sources are cooled in electronics packaging applications is the two-dimensional enclosure with discretely heated vertical wall (Fig. 2). The opposing wall serves as heat sink. Such a model is well suited for numerical simulation, and has been used in several studies [2–16]. In this and the following sections we explore the fundamental question of how to position a number of finite-size heat strips on one of the vertical walls. How many strips, and how should

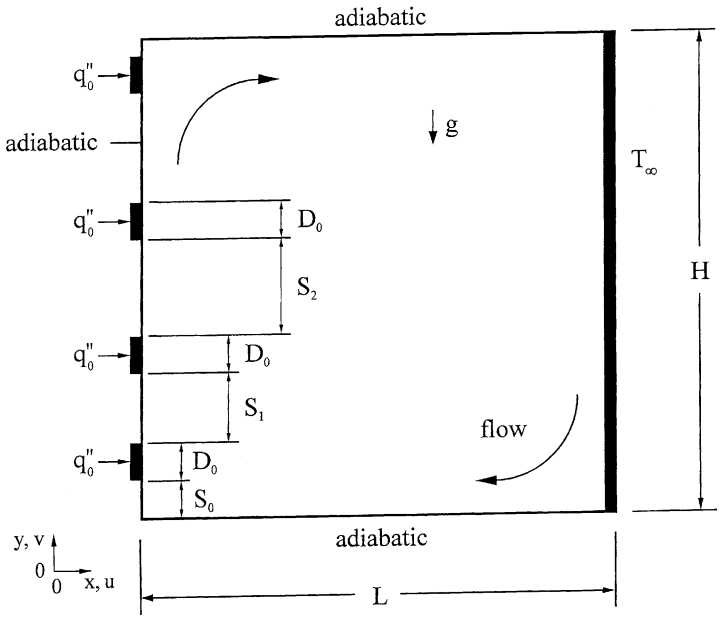

Fig. 2. Two-dimensional enclosure with discrete heat sources on one vertical wall.

they be interspaced? The systematic search for the optimal configuration is guided by the limiting case of the same problem, which was described analytically in the preceding sections.

The enclosure model is classical (e.g., Ref. [17, Chapter 5]), therefore we describe it briefly. The rectangular frame has the height H and horizontal dimension L, however, we set $L = H$ in order to be able to focus on the optimization of the multiple length scales of the vertical wall with distributed heating. The enclosure is filled with a newtonian fluid. Temperature variations are small when compared with the absolute temperature, and, consequently, we assume that the Boussinesq approximation is valid. In the Cartesian frame with the origin in the lower-left corner, the conservation equations for continuity, momentum and energy are

$$\frac{\partial u}{\partial x}+\frac{\partial v}{\partial y}=0 \tag{16}$$

$$\rho\left(u\frac{\partial u}{\partial x}+v\frac{\partial u}{\partial y}\right)=-\frac{\partial P}{\partial x}+\mu\nabla^2 u \tag{17}$$

$$\rho\left(u\frac{\partial v}{\partial x}+v\frac{\partial v}{\partial y}\right)=-\frac{\partial P}{\partial y}+\mu\nabla^2 v+\rho g\beta(T-T_0) \tag{18}$$

$$\rho c_p\left(u\frac{\partial T}{\partial x}+v\frac{\partial T}{\partial y}\right)=k\nabla^2 T \tag{19}$$

where $\nabla^2=\partial^2/\partial x^2+\partial^2/\partial y^2$.

5. Numerical formulation

The governing equations and boundary conditions are nondimensionalized by using the variables

$$(\tilde{x},\tilde{y},\widetilde{D}_0,\widetilde{S}_i)=\frac{(x,y,D_0,S_i)}{H} \tag{20}$$

$$(\tilde{u},\tilde{v})=\frac{(u,v)}{(\alpha/H)Ra_*^{1/2}Pr^{1/2}} \tag{21}$$

$$\widetilde{T}=\frac{T-T_\infty}{q_0''H/k} \tag{22}$$

$$\widetilde{P}=\frac{P}{(\mu\alpha/H^2)Ra_*^{1/2}Pr^{1/2}} \tag{23}$$

where Ra_* is the Rayleigh number based on the heat source strength,

$$Ra_*=\frac{g\beta q_0''H^4}{\alpha\nu k} \tag{24}$$

and $Pr=\nu/\alpha$. The nondimensional version of Eqs. (16)–(19) is

$$\frac{\partial\tilde{u}}{\partial\tilde{x}}+\frac{\partial\tilde{v}}{\partial\tilde{y}}=0 \tag{25}$$

$$\left(\frac{Ra_*}{Pr}\right)^{1/2}\left(\tilde{u}\frac{\partial\tilde{u}}{\partial\tilde{x}}+\tilde{v}\frac{\partial\tilde{u}}{\partial\tilde{y}}\right)=-\frac{\partial\widetilde{P}}{\partial\tilde{x}}+\nabla^2\tilde{u} \tag{26}$$

$$\left(\frac{Ra_*}{Pr}\right)^{1/2}\left(\tilde{u}\frac{\partial\tilde{v}}{\partial\tilde{x}}+\tilde{v}\frac{\partial\tilde{v}}{\partial\tilde{y}}\right)=-\frac{\partial\widetilde{P}}{\partial\tilde{y}}+\nabla^2\tilde{v}+\left(\frac{Ra_*}{Pr}\right)^{1/2}\widetilde{T} \tag{27}$$

$$(Ra_*Pr)^{1/2}\left(\tilde{u}\frac{\partial\widetilde{T}}{\partial\tilde{x}}+\tilde{v}\frac{\partial\widetilde{T}}{\partial\tilde{y}}\right)=\nabla^2\widetilde{T} \tag{28}$$

The flow boundary conditions are no slip ($\tilde{u}=\tilde{v}=0$) and no penetration along all internal surfaces. The right wall is isothermal at $\widetilde{T}=0$. The left wall has one or more heat strips of height $\widetilde{D}_0$. Each strip dissipates uniformly a dimensionless heat flux of $\tilde{q}=1$, which is defined later in Eq. (30). The top and bottom walls, and the wall sections ($\widetilde{S}_0$, $\widetilde{S}_1,\ldots$) that separate the $\widetilde{D}_0$ strips are adiabatic.

The Prandtl number was fixed at $Pr=0.7$. Numerical solutions for the velocity and temperature fields were generated by using a finite-element package [18]. The upwind formulation was used in order to handle the inherent instabilities associated with flow regions where convection is stronger than diffusion, and where there are large gradients in the flow variables. The finite-elements were quadrilateral with 9 nodes per element. The explicit appearance of the pressure terms in the momentum Eqs. (26) and (27) was eliminated by using the penalty function. In all the simulations the penalty parameter was fixed at 10^{-8}. The nonlinear equations resulting from the Galerkin finite-element discretization were solved using successive substitution, which was followed by the Newton–Raphson method. The convergence criteria used were

$$\frac{\|\mathbf{u}^{(n)}-\mathbf{u}^{(n-1)}\|}{\|\mathbf{u}^{(n)}\|}\leqslant 0.001,\quad \frac{\|\mathbf{R}(\mathbf{u}^{(n)})\|}{\|\mathbf{R}_0\|}\leqslant 0.001 \tag{29}$$

where $\mathbf{R}$, is the residual vector, $\mathbf{u}$ is the solution vector, and n is the iteration number.

Extensive grid refinement tests were performed before each group of simulations (e.g., Tables 1 and 2). The tests showed that the average heat flux from one heat source,

$$\tilde{q}=\frac{k(\partial T/\partial x)_{x=0}}{q_0''}=\frac{q''}{q_0''} \tag{30}$$

and the maximal temperature reached at any point on the wall

$$\widetilde{T}_{\max}=\frac{T_{\max}-T_\infty}{q_0''H/k} \tag{31}$$

are sufficiently insensitive to grid refinement in the entire Ra_* domain, $10^2\leqslant Ra_*\leqslant 10^6$. The selected grid had 101 nodes in both $\tilde{x}$ and $\tilde{y}$ directions. The grid was

Table 1
Grid refinement test for $\widetilde{D}_0 = 0.1$, $\widetilde{S}_0 = 0$, $Pr = 0.7$, $H/L = 1$ and $Ra_* = 10^2$

Mesh	Nodes	Elements	$\tilde{q}$	$\left\|\frac{\tilde{q}^i - \tilde{q}^{i+1}}{\tilde{q}^i}\right\|$	$\widetilde{T}_{\max}$	$\left\|\frac{\widetilde{T}^i_{\max} - \widetilde{T}^{i+1}_{\max}}{\widetilde{T}^i_{\max}}\right\|$
25×25	625	192	0.9335	–	0.235585	–
51×51	2601	725	0.9675	0.0364	0.237092	0.00639
75×75	5625	1517	0.9782	0.0110	0.237189	0.00041
101×101	10,201	2700	0.9848	0.0067	0.237203	0.00006
151×151	28,801	5925	0.9897	0.0049	0.237208	0.00002

Table 2
Grid refinement test for $\widetilde{D}_0 = 0.1$, $\widetilde{S}_0 = 0$, $Pr = 0.1$, $H/L = 1$ and $Ra_* = 10^6$

Mesh	Nodes	Elements	$\tilde{q}$	$\left\|\frac{\tilde{q}^i - \tilde{q}^{i+1}}{\tilde{q}^i}\right\|$	$\widetilde{T}_{\max}$	$\left\|\frac{\widetilde{T}^i_{\max} - \widetilde{T}^{i+1}_{\max}}{\widetilde{T}^i_{\max}}\right\|$
25×25	625	192	0.9498	–	0.104267	–
51×51	2601	725	0.9674	0.0185	0.104602	0.00321
75×75	5625	1517	0.9774	0.0103	0.104538	0.00061
101×101	10,201	2700	0.9841	0.0068	0.104531	0.00067
151×151	28,801	5925	0.9892	0.0052	0.104460	0.00067

nonuniform in the $\tilde{x}$ direction, with the narrower elements close to the vertical walls. The grid was uniform in $\tilde{y}$ direction. Tables 1 and 2 show the effect of the grid on $\tilde{q}$ and $\widetilde{T}_{\max}$ when there is only one heat source on the left wall of the enclosure. The same grid independence behavior was obtained for configurations with 2 and 3 heat sources, throughout the range $10^2 \leqslant Ra_* \leqslant 10^6$.

6. Optimal distribution of heat sources

In the numerical optimization of the distribution of heat sources, we searched not only for accurate optimal designs but also for the *patterns* in which the designs organize themselves. In the background was the question of whether the numerically optimized distributions approach in some ways the theoretical distribution anticipated in Eq. (6). If the answer is 'yes', then the theoretical distribution and the numerically documented 'pattern' represent a very useful *strategy* for future design.

Because of the potentially large number of geometric parameters that must be varied freely and optimized, we started with the simplest configuration. We then continued with configurations of stepwise increasing complexity. The simplest case is that where the left wall has a single heating patch of height $\widetilde{D}_0$. The variable geometric parameter is the position ($\widetilde{S}_0$) of this patch on the vertical wall. The parameters that are fixed for each group of simulations in which $\widetilde{S}_0$ varies are $\widetilde{D}_0$, Ra_* and, as we already mentioned, $H/L = 1$ and $Pr = 0.7$.

The objective in every case is to maximize the global thermal conductance of the enclosure, namely

$$C = \frac{Q'}{k(T_{\max} - T_\infty)} \tag{32}$$

where Q' is the total heat current through the source strip of height $\widetilde{D}_0$. The global conductance C is a dimensionless way of expressing the ratio of the total heat transfer rate Q' (fixed) divided by the largest temperature difference between a point on the hot wall and the cold wall.

Fig. 3 shows that C can be maximized by selecting the location of a single heat source ($\widetilde{S}_0$). In this particular case, the Rayleigh number is not very high ($Ra_* = 10^3$) and the optimal position of the heat source is nearly in the middle of the hot wall ($\widetilde{S}_{0,\text{opt}} = 0.45$). Selecting the value of $\widetilde{S}_0$ is critical because the C maximum is not flat.

Fig. 4 shows how the optimal location responds to changes in $\widetilde{D}_0$ and Ra_*. The optimal location migrates toward the starting corner of the left wall ($y = 0$) as Ra_* increases. It is there that the flow is most intense and the heat transfer coefficient the largest. The effect of source size on $\widetilde{S}_{0,\text{opt}}$ is weak. It is stronger in Fig. 5, which shows the maximized global conductance that corresponds to the optimized single-source locations presented in Figs. 3 and 4. The Ra_* value has an interesting effect on $C_{\max}$: it is only when Ra_* exceeds the order of 10^4 that $C_{\max}$ increases with Ra_* (proportionally with $Ra_*^{0.18}$ when $Ra_* \sim 10^6$). At lower Rayleigh numbers, thermal diffusion reaches from the side walls to the core of the enclosure.

The next configuration that we optimized had two heat sources, hence, two degrees of freedom: the spacings $\widetilde{S}_0$ and $\widetilde{S}_1$. We performed the optimization in two nested loops, by considering all the possible combinations of $\widetilde{S}_0$ and $\widetilde{S}_1$. In the inner loop, we fixed $\widetilde{S}_0$,

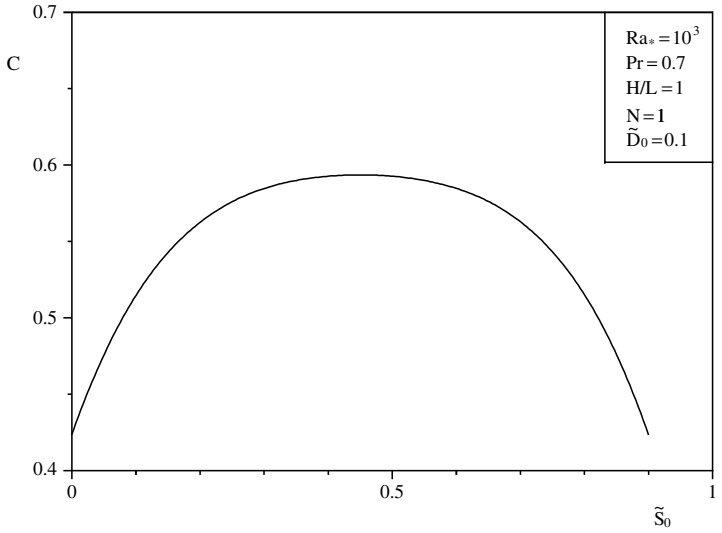

Fig. 3. The maximization of the global conductance when only one heat source is present.

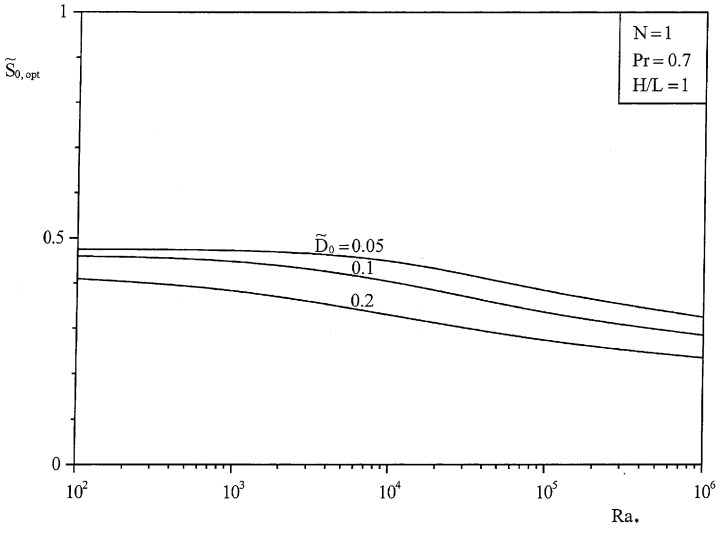

Fig. 4. The effect of Rayleigh number and heat source size on the optimal location of the single heat source.

maximized C with respect to $\widetilde{S}_1$, and obtained $C_{\max}$. Next, we repeated the procedure and maximized $C_{\max}$ with respect to $\widetilde{S}_0$, and obtained the twice-maximized conductance C_{2m}.

The optimal spacings $(\widetilde{S}_0, \widetilde{S}_1)_{opt}$ are reported in Fig. 6. Qualitatively, they reveal the same trends as the location of the single-source in Fig. 4. The migration of the two heat sources when Ra_* increases is an illustration of optimal distribution of imperfection (constructal design): the heat sources arrange themselves in the stronger flow regions, such that their hot spots are suppressed the most.

The maximized global conductances that correspond to the configurations of Fig. 6 are reported in Fig. 7. Here we see the same behavior as in Fig. 5, especially the boundary layer effect that sets in when Ra_* exceeds 10^4. The important aspect of Fig. 7 is that each curve shows a higher conductance than the curve for the same Ra_* and $\widetilde{D}_0$ in Fig. 5.

Another important aspect of the maximization of global performance is observed when the total heated area is held constant. By fixing $N\widetilde{D}_0 = 0.1$ and $Ra_* = 10^2$, for example, Fig. 5 shows that $C_{\max} = 0.5927$ when only one heat source of height $\widetilde{D}_0 = 0.1$ is present.

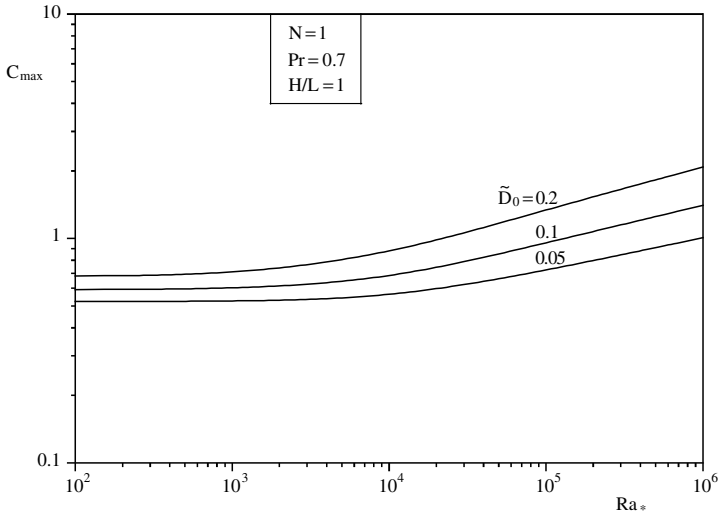

Fig. 5. The maximized global conductance that corresponds to the optimized location of the single heat source.

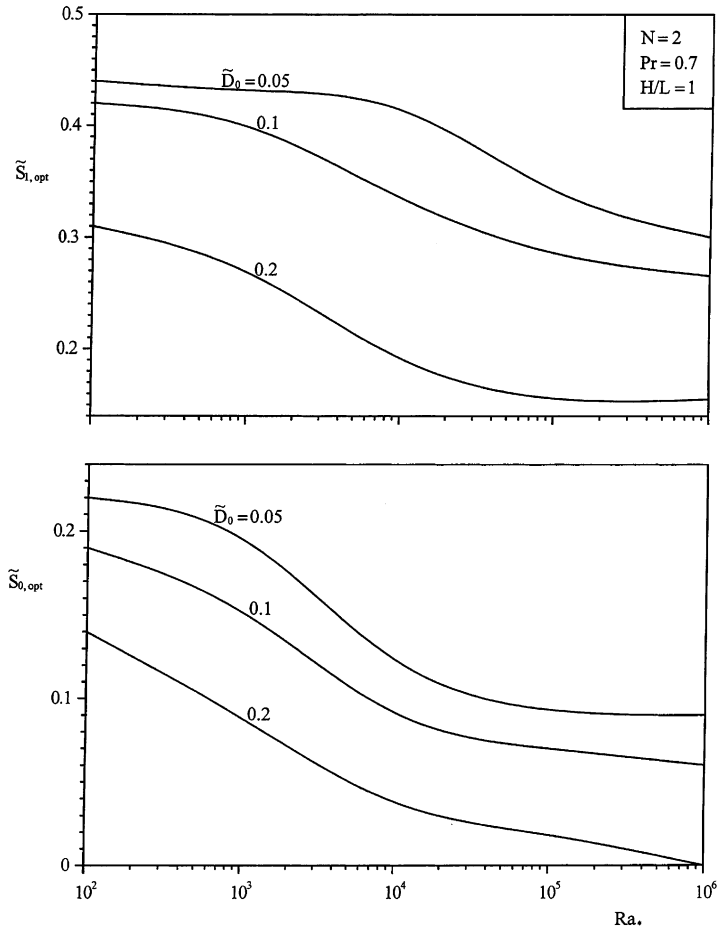

Fig. 6. The optimal locations of two heat sources.

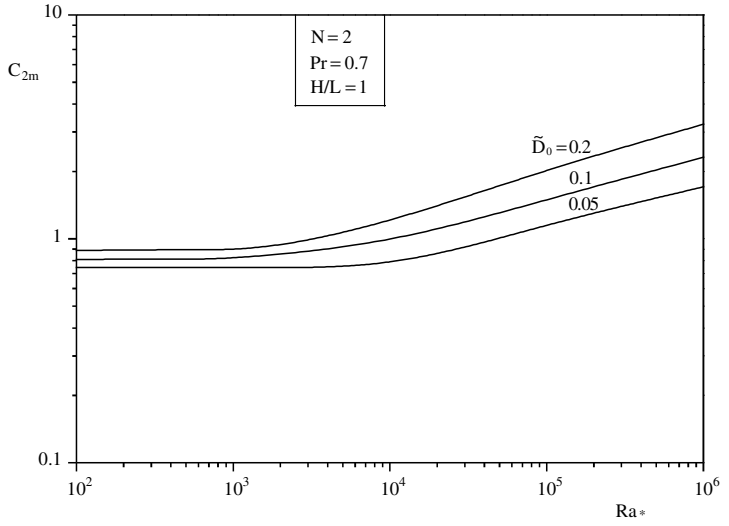

Fig. 7. The maximized global conductance that corresponds to the optimized placement of two heat sources.

For the same fixed heated area, Fig. 7 shows that $C_{2m} = 0.7447$ if two identical sources of height $\widetilde{D}_0 = 0.05$ are optimally placed on the left wall. The difference between the conductances represents an improvement in global performance of approximately 25%. The same relative improvement is observed for $Ra_* = 10^3$. In the range $10^4 \leqslant Ra_* \leqslant 10^6$ the increasing rate is constant and equal to approximately 20%. The same calculations can be done for $N\widetilde{D}_0 = 0.2$, constant. In this case, the benefits associated with the splitting of one optimally placed heat source of height $\widetilde{D}_0 = 0.2$ into two optimally placed heat sources of height $\widetilde{D}_0 = 0.1$ is equal to ≈20% and 10% in the ranges $10^2 \leqslant Ra_* \leqslant 10^3$ and, respectively, $10^4 \leqslant Ra_* \leqslant 10^6$. The existence of these two distinct regions with different levels of performance is due to the fact that at low Rayleigh numbers ($10^2 \leqslant Ra_* \leqslant 10^3$) the flow is weak, and, as we increase the number of optimally placed heat sources $\widetilde{T}_{max}$ decreases, and consequently C increases. At high Rayleigh numbers ($10^4 \leqslant Ra_* \leqslant 10^6$) the influence of the number of heat sources on the global performance for a fixed heated area is less important, because the flow is much stronger and more able to cool down the left wall.

The next configuration on the ladder of increasing complexity is the wall with three heat sources. The procedure of optimizing the geometry is the same, except that now the geometry has three degrees of freedom: $\widetilde{S}_0$, $\widetilde{S}_1$ and $\widetilde{S}_2$. The optimized spacings are reported in Fig. 8

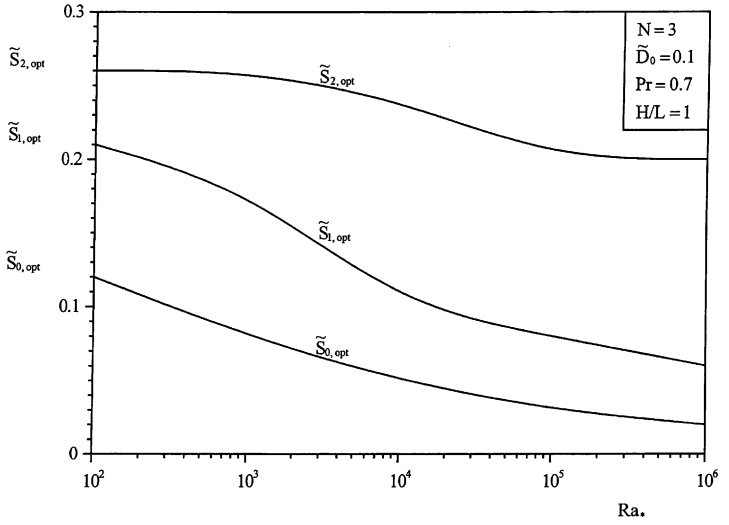

Fig. 8. The optimal locations of three heat sources.

for the heat source size $\widetilde{D}_0 = 0.1$. The increasing Ra_* value has the effect of pushing the heat sources towards the starting corner of the hot wall ($y = 0$). The trailing heat source is least sensitive to this influence: see $\widetilde{S}_{2,\mathrm{opt}}$, which is relatively stationary in the 0.2–0.25 range.

The effect of using three heat sources is to augment further the thermal contact between the wall and the fluid. Fig. 9 shows the maximized global conductance for three sources ($C_{3\mathrm{m}}$) next to the corresponding curves for two heat sources ($C_{2\mathrm{m}}$, Fig. 7) and one heat source ($C_{\max}$, Fig. 5). This comparison is for one heat source size, $\widetilde{D}_0 = 0.1$. Note the occurrence of diminishing returns: the conductance increase registered from $N = 2$ to 3 is smaller than the increase obtained as N changes from 1 to 2.

Another interesting effect becomes visible if we repeat the three-source optimization of Figs. 8 and 9 but use a larger heat source size. Fig. 10 shows the results for the optimal spacings when $\widetilde{D}_0 = 0.2$. Unlike in Fig. 8, optimal spacings for $\widetilde{S}_0$ and $\widetilde{S}_1$ are found only if Ra_* is less than 3×10^3 and 5×10^3, respectively. At greater Ra_* values, $Ra_* > 5 \times 10^5$, the largest C values belong to

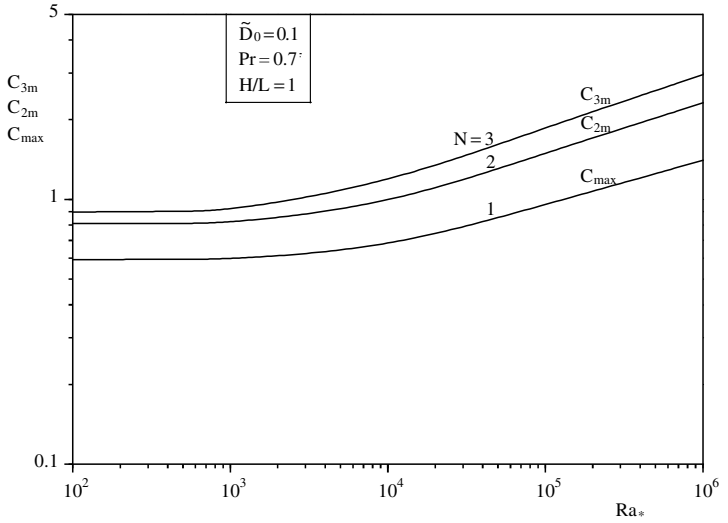

Fig. 9. The effect of the number of discrete heat sources on the maximized global conductance.

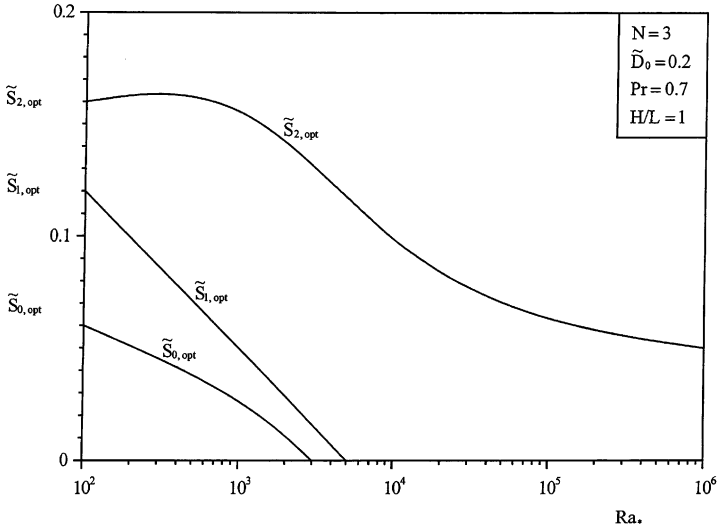

Fig. 10. The optimal location of three heat sources when the source size is larger ($\widetilde{D}_0 = 0.2$).

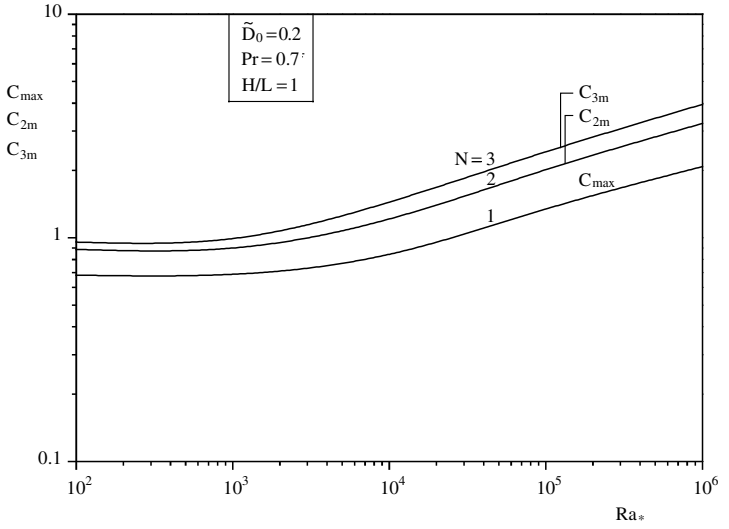

Fig. 11. The effect of N on the maximized global conductance when $\widetilde{D}_0 = 0.2$.

designs with $\widetilde{S}_0 = \widetilde{S}_1 = 0$, which represent a continuous heating strip of size $2\widetilde{D}_0$ placed in the starting corner of the hot wall. The coalescence of discrete heat sources at the start of the boundary layer is consistent with the discussion of the height $y_0 (= N_0 D_0)$ in Section 3. Coalescence occurs as Ra_* increases.

The maximized thermal conductance summary for $\widetilde{D}_0 = 0.2$ is presented in Fig. 11. This summary is similar to Fig. 9. The diminishing returns associated with increasing N are once again evident.

7. Conclusions

In this paper we considered the fundamental problem of how to arrange a number of discrete heat sources on a vertical wall with natural convection. In the first part of the paper we showed analytically that an optimal arrangement exists. The spacings between heat sources are not uniform, and depend on the Rayleigh number. The optimal distribution of heat sources leads to maximal global performance—the minimal global thermal resistance between the wall and the fluid.

Heat sources must be positioned closer together when they reside near the start of the boundary layer. There is a region near the tip of the boundary layer ($0 < y < y_0$) where the heat sources must be positioned flush against each other. Above y_0, the spacing between heat sources increases with altitude. In summary, Eq. (11) shows that as the Rayleigh number increases, the heat sources migrate toward the tip of the boundary layer. Contrary to the results of Ref. [12], the optimal arrangement is not described by a constant ratio between the center-to-center distance between heat sources, but by a function that depends strongly on the Rayleigh number and the heat source strength D_0.

The theoretical trends were verified numerically in the second part of the paper, where the heat sources were mounted inside the left wall of a square enclosure. The numerical study covered not only the high-Ra_* regime with distinct boundary layers, but also the low-Ra_* regime where boundary layers are not distinct. For example, when $Ra_* < 10^4$ the maximized global conductance (C_{max}, C_{2m}, or C_{3m}) is practically independent of Ra_*. On the other hand, when $Ra_* > 10^4$, the maximized global conductance increases in proportion with approximately $Ra_*^{0.18}$.

Figs. 9 and 11 showed that the maximized global conductance increases as more heat sources are added, but that the rate of increase slows down. Diminishing returns is an important characteristic of optimized complex structures. It is also an important consideration in practice: how much optimization and complexity is enough? Future numerical work may extend the coverage of this study to enclosures with more than three discrete heat sources. In this direction, one could also explore the overlap between numerically optimized arrangements and the analytical design rules of Sections 2 and 3.

Acknowledgements

A.K. da Silva acknowledges the support received from Conselho Nacional de Desenvolvimento Cientifico e Tecnológico (CNPq) Brazil. A. Bejan's work was supported by a grant from the National Science Foundation.

References

[1] A. Bejan, Shape and Structure, from Engineering to Nature, Cambridge University Press, Cambridge, UK, 2000.
[2] C.J. Ho, J.Y. Chang, A study of natural-convection heat-transfer in a vertical rectangular enclosure with 2-dimensional discrete heating—effect of aspect ratio, Int. J. Heat Mass Transfer 37 (1994) 917–925.
[3] M.M. Ganzarolli, L.F. Milanez, Natural convection in rectangular enclosures heated from below and symmetrically cooled from the sides, Int. J. Heat Mass Transfer 38 (1995) 1063–1073.
[4] T.J. Heindel, S. Ramadhyani, F.P. Incropera, Laminar natural convection in a discretely heated cavity. 1. Assessment of three-dimensional effects, J. Heat Transfer 117 (1995) 902–909.
[5] T.J. Heindel, F.P. Incropera, S. Ramadhyani, Laminar natural convection in a discretely heated cavity. 2. Comparisons of experimental and theoretical results, J. Heat Transfer 117 (1995) 910–917.
[6] T.J. Heindel, S. Ramadhyani, F.P. Incropera, Conjugate natural convection from an array of discrete heat sources. 1. Two and three-dimensional model validation, Int. J. Heat Fluid Flow 16 (1995) 501–510.
[7] M. Fujii, S. Gima, T. Tomimura, X. Zhang, Natural convection to air from an array of vertical parallel plates with discrete and protruding heat sources, Int. J. Heat Fluid Flow 17 (1996) 483–490.
[8] T.J. Heindel, F.P. Incropera, S. Ramadhyani, Enhancement of natural convection heat transfer from an array of discrete heat sources, Int. J. Heat Mass Transfer 39 (1996) 479–490.
[9] H.Y. Wang, F. Penot, J.B. Saulnier, Numerical study of a buoyancy-induced flow along a vertical plate with discretely heated integrated circuit packages, Int. J. Heat Mass Transfer 40 (1997) 1509–1520.
[10] S.K.W. Tou, C.P. Tso, X. Zhang, 3-D numerical analysis of natural convective liquid cooling of a 3×3 heater array in rectangular enclosures, Int. J. Heat Mass Transfer 42 (1999) 3231–3244.
[11] I. Sezai, A.A. Mohamad, Natural convection from a discrete heat source on the bottom of a horizontal enclosure, Int. J. Heat Mass Transfer 43 (2000) 2257–2266.
[12] Y. Liu, N. Phan-Thien, An optimum spacing problem for three chips mounted on a vertical substrate in an enclosure, Numer. Heat Transfer A 37 (2000) 613–630.
[13] Q.H. Deng, G.-F. Tang, Y. Li, A combined temperature scale for analyzing natural convection in rectangular enclosures with discrete wall heat sources, Int. J. Heat Mass Transfer 45 (2002) 3437–3446.
[14] Q.H. Deng, G.F. Tang, Y.G. Li, M.Y. Ha, Interaction between discrete heat sources in horizontal natural convection enclosures, Int. J. Heat Mass Transfer 45 (2002) 5117–5132.
[15] E. Yu, Y. Joshi, Heat transfer enhancement from enclosure discrete components using pin-fin heat sinks, Int. J. Heat Mass Transfer 45 (2002) 4957–4966.
[16] S.K.W. Tou, X.F. Zhang, Three-dimensional numerical simulation of natural convection in an inclined liquid-filled enclosure with an array of discrete heaters, Int. J. Heat Mass Transfer 46 (2003) 127–138.
[17] A. Bejan, Convection Heat Transfer, second ed., Wiley, New York, 1995, p. 176.
[18] FIDAP Manual, Fluid Dynamics International, Inc., Evanston, IL, 1998.